

# Supplementary Information

## Efficient and bright warm-white electroluminescence from lead-free metal halides

Hong Chen<sup>1†</sup>, Lin Zhu<sup>1†</sup>, Chen Xue<sup>2†</sup>, Pinlei Liu<sup>1</sup>, Xuerong Du<sup>1</sup>, Kaichuan Wen<sup>1</sup>, Hao Zhang<sup>1</sup>, Lei Xu<sup>1</sup>, Chensheng Xiang<sup>3</sup>, Chen Lin<sup>4</sup>, Minchao Qin<sup>5</sup>, Jing Zhang<sup>6</sup>, Tao Jiang<sup>1</sup>, Chang Yi<sup>1</sup>, Lu Cheng<sup>1</sup>, Chenglong Zhang<sup>1</sup>, Pinghui Yang<sup>1</sup>, Meiling Niu<sup>1</sup>, Wenjie Xu<sup>1</sup>, Jingya Lai<sup>1</sup>, Yu Cao<sup>1,2</sup>, Jin Chang<sup>1</sup>, He Tian<sup>3</sup>, Yizheng Jin<sup>4</sup>, Xinhui Lu<sup>5</sup>, Lang Jiang<sup>6</sup>, Nana Wang<sup>1\*</sup>, Wei Huang<sup>1,2\*</sup> and Jianpu Wang<sup>1\*</sup>

<sup>1</sup>Key Laboratory of Flexible Electronics (KLOFE) & Institute of Advanced Materials (IAM), Nanjing Tech University (NanjingTech), 30 South Puzhu Road, Nanjing 211816, China

<sup>2</sup>Shaanxi Institute of Flexible Electronics (SIFE), Xi'an Institute of Biomedical Materials & Engineering (IBME), Northwestern Polytechnical University (NPU), 127 West Youyi Road, Xi'an 710072, China

<sup>3</sup>China Center of Electron Microscope, State Key Laboratory of Silicon Material, School of Material Science & Engineering, Zhejiang University, Hangzhou 310027, China

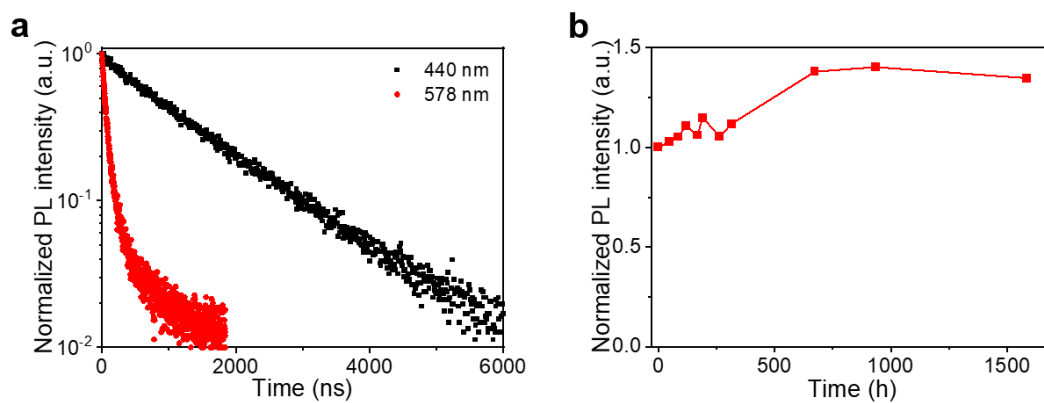
<sup>4</sup>Center for Chemistry of High-Performance and Novel Materials, State Key Laboratory of Silicon Materials, and Department of Chemistry, Zhejiang University, Hangzhou 310027, China

<sup>5</sup>Department of Physics, The Chinese University of Hong Kong, Shatin 999077, Hong Kong, China

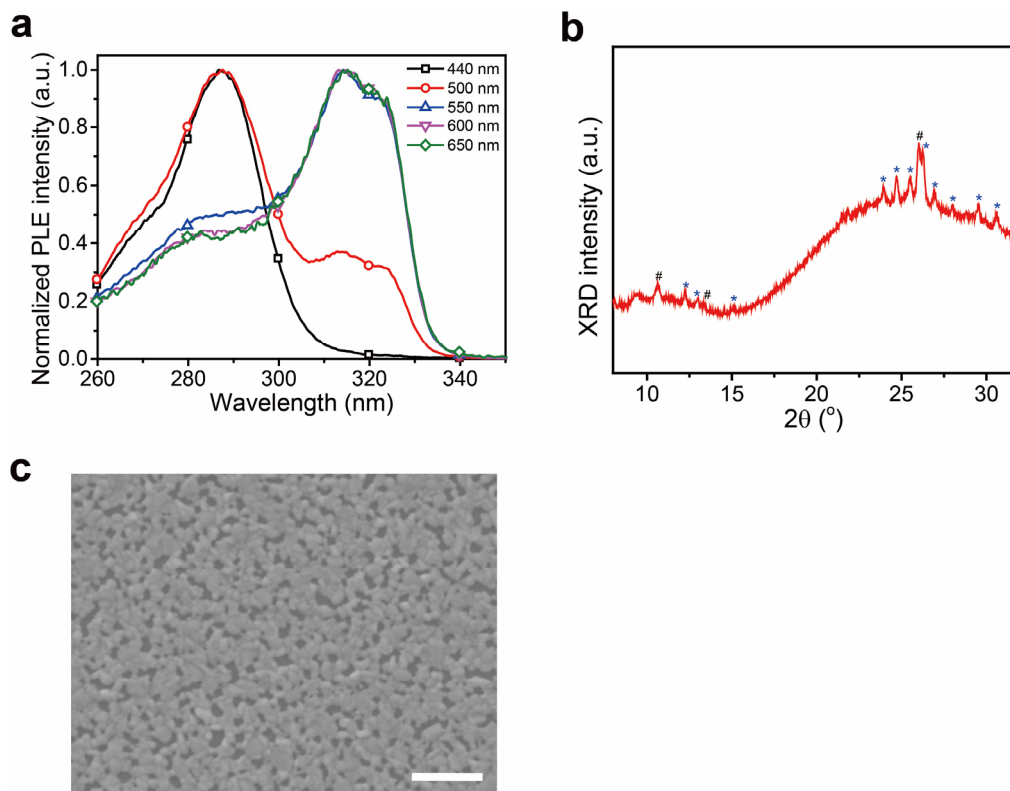
<sup>6</sup>Beijing National Laboratory for Molecular Sciences, Key Laboratory of Organic Solids, Institute of Chemistry, Chinese Academy of Sciences, Beijing 100190, China

Corresponding authors: Prof. Nana Wang (iamnawang@njtech.edu.cn); Prof. Wei Huang (iamwhuang@nwpu.edu.cn); Prof. Jianpu Wang (iamjpwang@njtech.edu.cn).

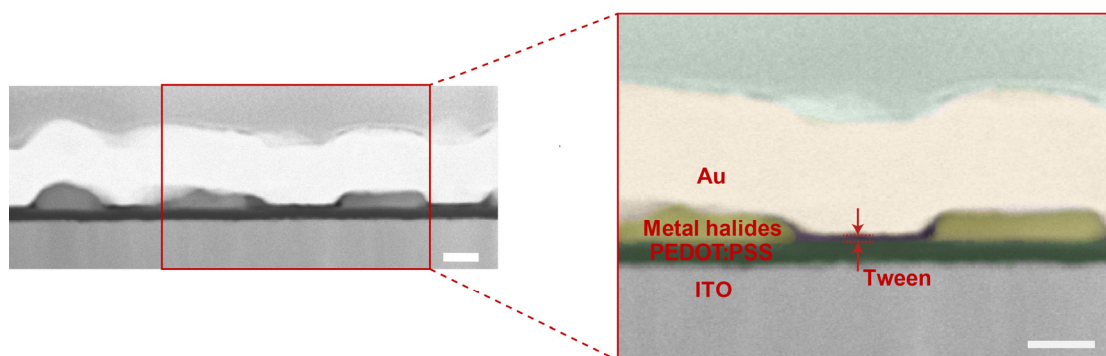
†These authors contributed equally to this work.



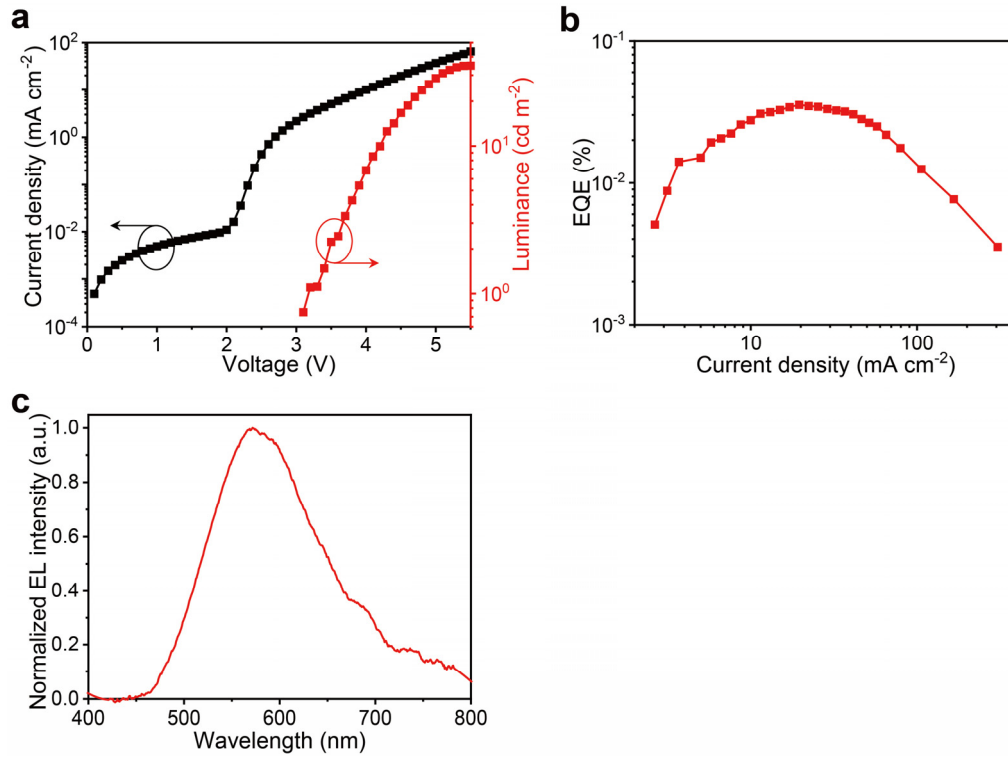
**Supplementary Figure 1. Characterizations of cesium-copper-iodide films with Tween.** **a**, Time-resolved PL decay curves. **b**, Evolution of PL intensity of the unencapsulated film stored in air with different time.



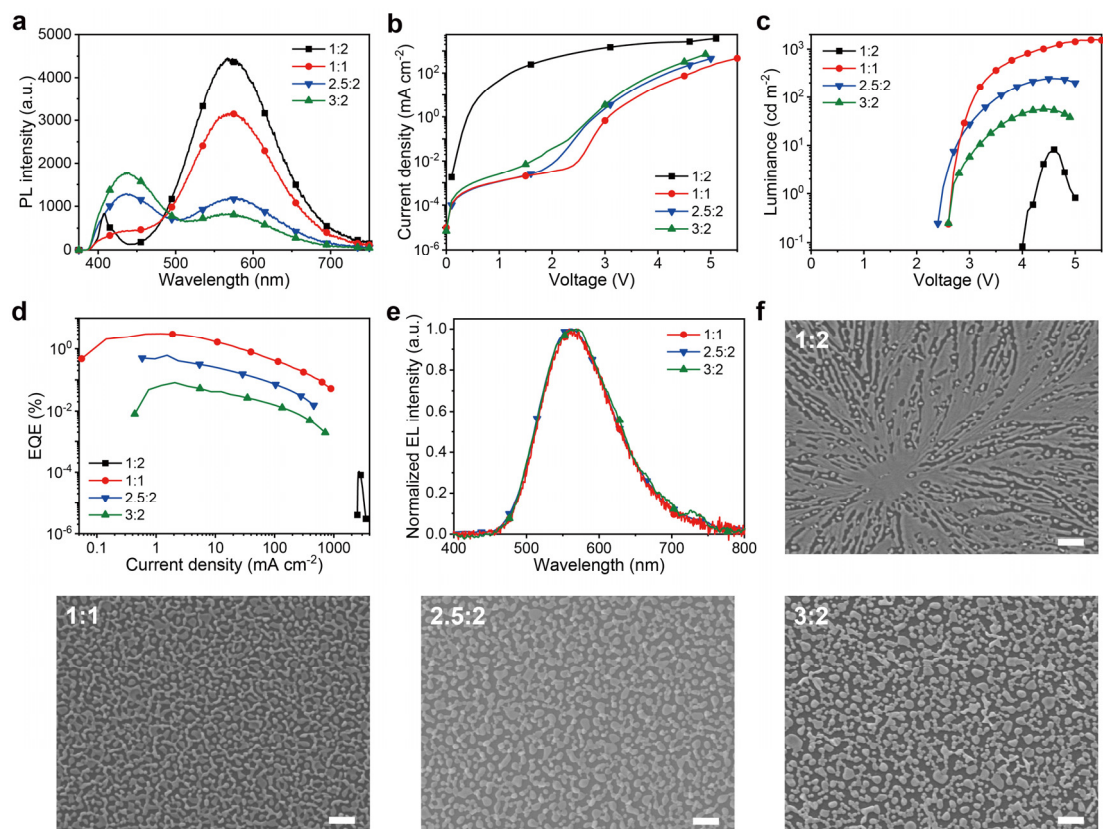
**Supplementary Figure 2. Characterizations of cesium-copper-iodide films without Tween.** **a**, Normalized PLE spectra at various emission wavelengths. **b**, XRD pattern. **c**, SEM image. Scale bar, 1  $\mu\text{m}$ .



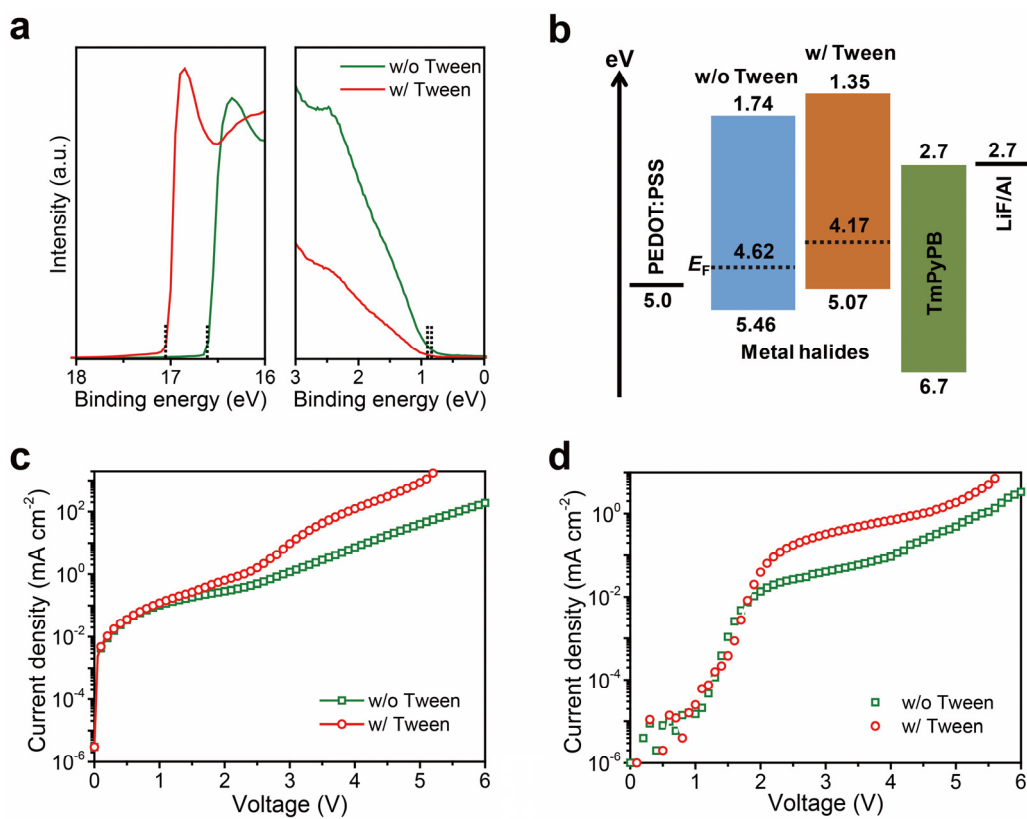
**Supplementary Figure 3. Cross-sectional STEM image of the metal halide film (Scale bar, 100 nm).** The STEM measurement was performed on a sample with structure of ITO/PEDOT:PSS/metal halides/Au. The layers in the right panel were tinted. Tween lies between the discrete cesium-copper-iodide crystallites, with a thickness of  $\sim 9$  nm.



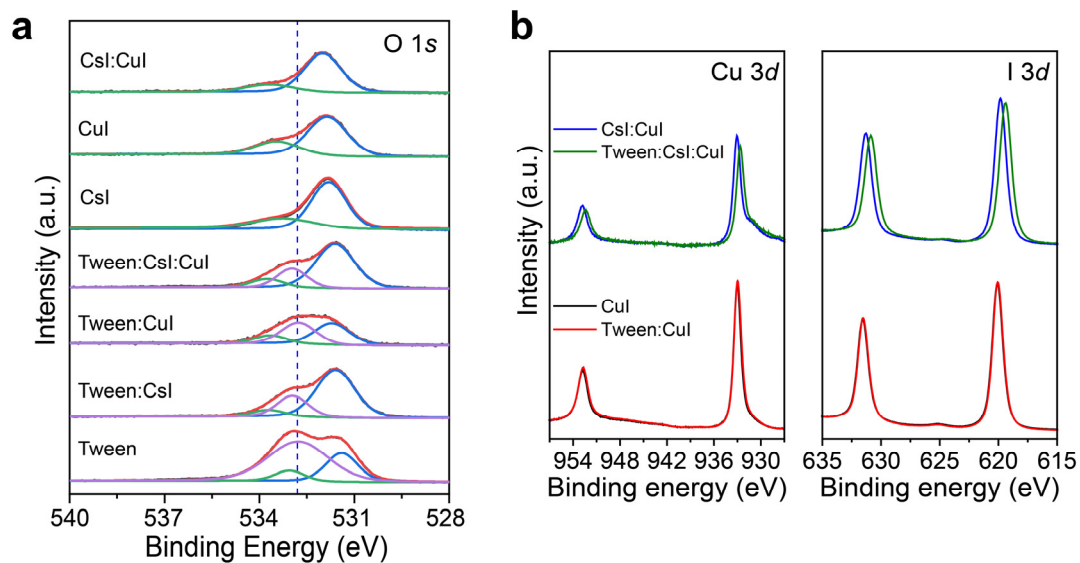
**Supplementary Figure 4. Characterizations of devices fabricated from the cesium-copper-iodide films without Tween. a**, Dependence of current density and luminance on the driving voltage. **b**, EQE versus current density. **c**, EL spectrum.



**Supplementary Figure 5. Characterizations of films and devices fabricated from different ratios of CsI:CuI with Tween. a**, PL spectra. **b**, Dependence of current density on the driving voltage. **c**, Dependence of luminance on the driving voltage. **d**, EQE versus current density. **e**, EL spectra. **f**, SEM images. Scale bar, 1  $\mu\text{m}$ .

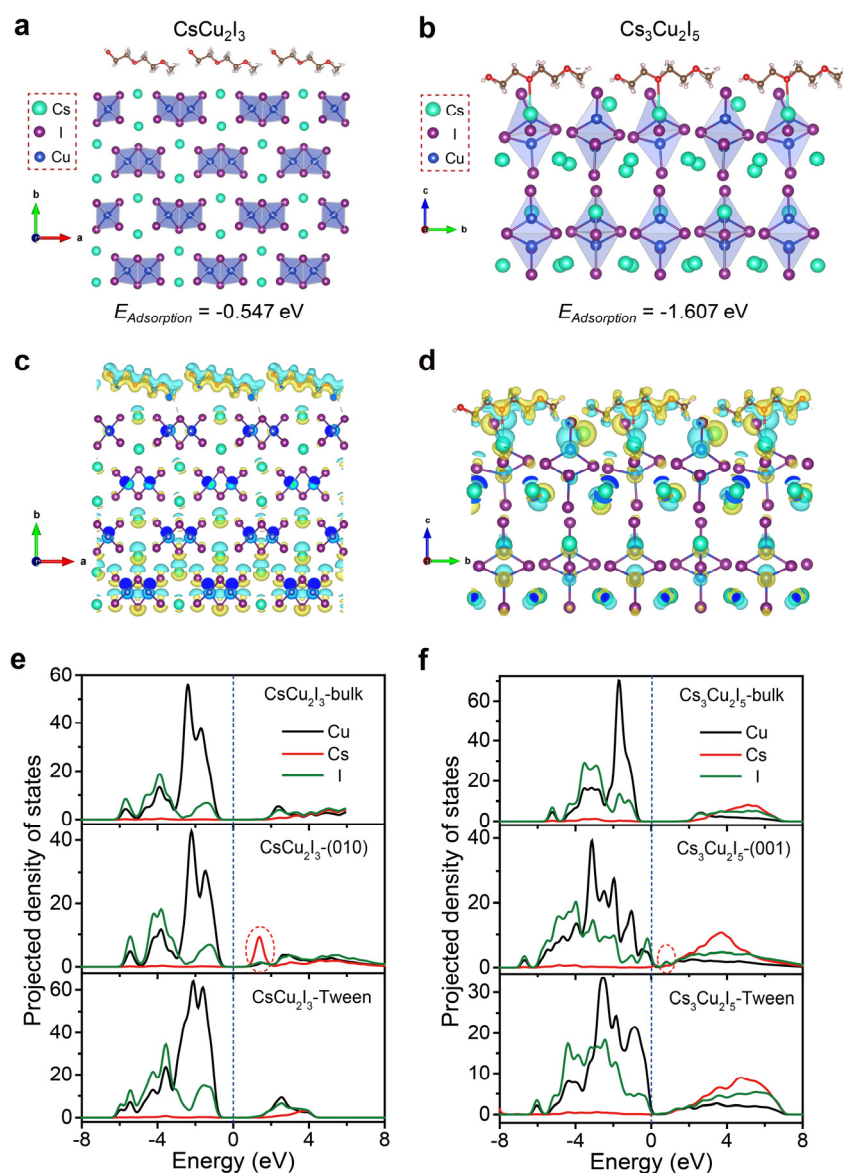


**Supplementary Figure 6. Electronic properties of cesium-copper-iodide films. a,** UPS spectra. After adding Tween, the valence band of cesium-copper-iodide film was changed from 5.46 to 5.07 eV. **b,** Schematic flat-band energy level diagram. The energy level values of cesium copper iodides were measured by UPS. **c,** J-V characterization of single-hole device with a structure of ITO/PEDOT:PSS/metal halide/TFB/MoO<sub>3</sub>/Au. **d,** J-V characterization of single-electron device with a structure of ITO/SnO<sub>2</sub>/PEIE/metal halide/TmPyPB/LiF/Al.

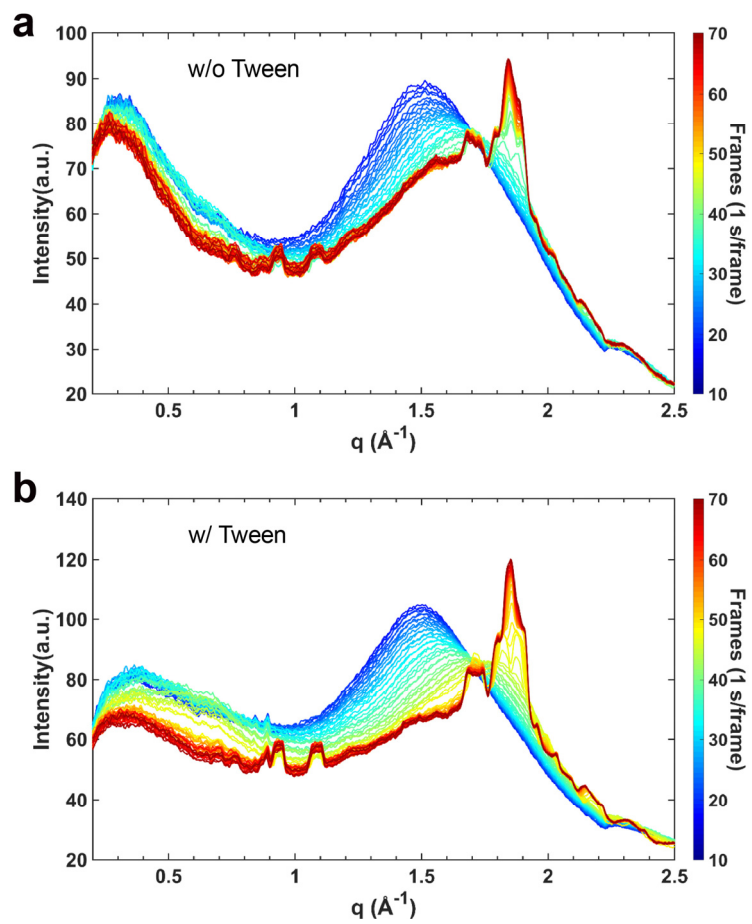


**Supplementary Figure 7. XPS spectra.** **a**, O 1s spectra. The O 1s lines were decomposed into two or three peaks. The red lines represent the raw data, while the blue, green lines represent the PEDOT:PSS and the purple lines represent the Tween. It shows that the peak of C=C-O group in PEDOT:PSS located at  $\sim 531.5$  eV<sup>1,2</sup> shifts to 531.9 eV in the samples with CsI or CuI, which indicates that the PEDOT:PSS substrate has a strong coupling with CsI, CuI, and CsI:CuI films. But the Tween additive can reduce this interaction, which shows the corresponding C=C-O peak locating at  $\sim 531.5$  eV. The peak at  $\sim 532.8$  eV assigned to the oxygen of Tween has no shift after the inclusion of CuI, but shifts to higher binding energy in Tween:CsI sample. **b**, Cu 3d and I 3d spectra of CuI, Tween:CuI, CsI:CuI and Tween:CsI:CuI films.

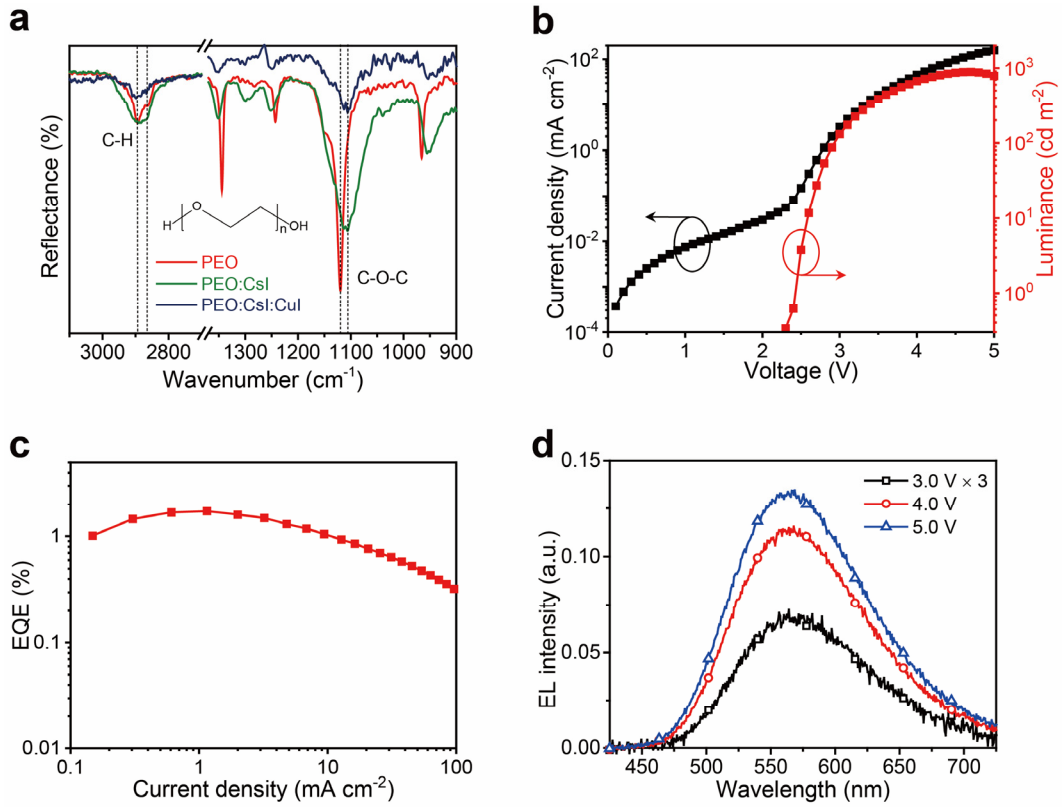




**Supplementary Figure 8. Calculations of the interaction between cesium copper iodides and Tween.** **a-b**, Optimized structures of CsCu<sub>2</sub>I<sub>3</sub> (010)-additive (a) and Cs<sub>3</sub>Cu<sub>2</sub>I<sub>5</sub> (001)-additive (b), with listed binding energy between the free additive and the crystalline surfaces. **c-d**, Charge density differences ( $\Delta\rho = \rho_{(crystal/additive)} - \rho_{crystal} - \rho_{additive}$ ) of the CsCu<sub>2</sub>I<sub>3</sub> (010)-additive (c) and Cs<sub>3</sub>Cu<sub>2</sub>I<sub>5</sub> (001)-additive (d). The yellow and cyan regions indicate charge accumulation and charge depletion, respectively. **e-f**, Calculated projected density of states of the CsCu<sub>2</sub>I<sub>3</sub> bulk, with Cs<sup>+</sup> exposed on the (010) facet and additive passivated CsCu<sub>2</sub>I<sub>3</sub> (e) and those of the Cs<sub>3</sub>Cu<sub>2</sub>I<sub>5</sub> bulk, the (001) facet with Cs<sup>+</sup> exposure and the additive passivated Cs<sub>3</sub>Cu<sub>2</sub>I<sub>5</sub> (f). The Fermi levels are highlighted by the blue dash lines. The copper-based compounds with crystalline facets exposed with Cs<sup>+</sup> create a sub-gap state highlighted by the red circles.



Supplementary Figure 9. Time-resolved GIWAXS profiles of cesium-copper-iodide films. **a**, Without Tween. **b**, With Tween.



**Supplementary Figure 10. Optoelectronic characteristics of the devices based on PEO.** **a**, FTIR spectra. After adding PEO to CsI, the  $1120 \text{ cm}^{-1}$  peak ascribed to C-O-C stretching vibration of PEO is shifted to  $1106 \text{ cm}^{-1}$ , which is similar in the PEO:CsI:CuI sample. Inset, the structure of the PEO molecule. **b**, Dependence of current density and luminance on the driving voltage. **c**, EQE versus current density. The PEO-based devices reach a peak EQE of 1.7% and a maximum luminance of  $890 \text{ cd m}^{-2}$ , respectively. **d**, EL spectra at different voltages.

**Supplementary Table 1. Comparison of our device with reported white metal halide LEDs.**

Emitter	EL peak (nm)	Maximum luminance (cd m <sup>-2</sup> )	Peak EQE (%)	Reference
CsPbBr <sub>x</sub> Cl <sub>3-x</sub> +MEH:PPV	470, 560	~150 <sup>†</sup>	-	3
PA <sub>2</sub> CsPb <sub>2</sub> I <sub>7</sub> +CsPb(Br/Cl) <sub>3</sub>	493, 693	-	0.22	4
MAPb(Br <sub>0.6</sub> Cl <sub>0.4</sub> ) <sub>3</sub> +organic compound	~500, 700	~14 <sup>†</sup>	~0.001	5
(C <sub>6</sub> H <sub>5</sub> C <sub>2</sub> H <sub>4</sub> NH <sub>3</sub> ) <sub>2</sub> PbCl <sub>2</sub> Br <sub>2</sub>	~475 <sup>†</sup>	~70	-	6
Cs <sub>2</sub> Ag <sub>0.60</sub> Na <sub>0.40</sub> InCl <sub>6</sub>	~559 <sup>†</sup>	~50 <sup>†</sup>	-	7
CsCu <sub>2</sub> I <sub>3</sub> +mCP	~554	~14 <sup>†</sup>	~0.15 <sup>†</sup>	8
Tween-(Cs <sub>3</sub> Cu <sub>2</sub> I <sub>5</sub> :CsCu <sub>2</sub> I <sub>3</sub> )	565	1570	3.1	This work

<sup>†</sup>These data were estimated from the figures in refs <sup>3,5-8</sup>.

### Supplementary References:

1. Mengistie, D. A., Ibrahim, M. A., Wang, P.-C. & Chu, C.-W. Highly conductive PEDOT:PSS treated with formic acid for ITO-free polymer solar cells. *ACS Appl. Mater. Interfaces* **6**, 2292–2299 (2014).
2. Fan, Z., Li, P., Du, D. & Ouyang, J. Significantly enhanced thermoelectric properties of PEDOT:PSS films through sequential post-treatments with common acids and bases. *Adv. Energy Mater.* **7**, 1602116 (2017).
3. Yao, E.-P. *et al.* High-brightness blue and white LEDs based on inorganic perovskite nanocrystals and their composites. *Adv. Mater.* **29**, 1606859 (2017).
4. Mao, J. *et al.* All-perovskite emission architecture for white light-emitting diodes. *ACS Nano* **12**, 10486–10492 (2018).
5. Chang, C.-Y. *et al.* Perovskite white light-emitting diodes based on a molecular blend perovskite emissive layer. *J. Mater. Chem. C* **7**, 8634–8642 (2019).
6. Cai, P., Wang, X., Seo, H. J. & Yan, X. Bluish-white-light-emitting diodes based on two-dimensional lead halide perovskite  $(\text{C}_6\text{H}_5\text{C}_2\text{H}_4\text{NH}_3)_2\text{PbCl}_2\text{Br}_2$ . *Appl. Phys. Lett.* **112**, 153901 (2018).
7. Luo, J. *et al.* Efficient and stable emission of warm-white light from lead-free halide double perovskites. *Nature* **563**, 541–545 (2018).
8. Roccanova, R. *et al.* Bright luminescence from nontoxic  $\text{CsCu}_2\text{X}_3$  ( $\text{X} = \text{Cl}, \text{Br}, \text{I}$ ). *ACS Mater. Lett.* **1**, 459–465 (2019).